Electrolyte Motion Induced Salt Inhomogeneity – A Novel Aging Mechanism in Large-Format Lithium-Ion Cells

Supporting information

Sophie Solchenbach[a,#], Camilla Tacconis, Aurora Gomez Martin[a], Verena Peters[a], Lea Wallisch[a], Anna Stanke[a], Johanna Hofer[a], Diemo Renz[a], Burkhard Lewerich[a], Georg Bauer[a], Moritz Wichmann[a], Daniel Goldbach[a], Alexander Adam[a], Markus Spielbauer[a], Peter Lamp[a], Johannes Wandt[a,b,#]

[a]BMW AG, 80788 Munich, Germany

[b]University of Agder, Grimstad, Norway

Table of content

Calculation of pore filling ratio

The pore filling ratio *PFR* as defined in equation 1) is similar to pore filling ratio definitions used in previous studies,[1,2] but our pore filling ratio also considers i) the SOC-dependency due to the reversible volume change of active materials, ii) the SEI volume, iii) the (largely irreversible) electrode expansion during initial cell formation (the "real" jelly roll volume after electrode expansion is determined from CT-images, rather than using pristine electrode volumes before cell formation), and iv) the loss of liquid electrolyte during cell formation. The calculation of the SOC-dependent pore volume V_{Pore} follows a general logic similar to the approaches developed by Pegel et al.[3] and Vidal et al.[4] and will be described in more detail in a manuscript which is currently under preparation. Here, we briefly describe the FEC reduction model we used to estimate the SEI volume and the loss of liquid electrolyte volume during initial cell formation.

Determination of $Q_{\mathrm{Irrev.SEI}}$. - From half-cell measurements we determined the irreversible capacity for the graphite/silicon-composite anode active material in combination with the same FEC-containing electrolyte which is associated with SEI formation. This $Q_{\mathrm{Irrev.SEI}}$ is not fully identical to the irreversible capacity that is observed in a full cell $Q_{\mathrm{Irrev.FullCell}}$ as the discharge in a full cell is partially terminated by the cathode (therefore $Q_{\mathrm{Irrev.SEI}} < Q_{\mathrm{Irrev.FullCell}}$). For our combination of anode active material and electrolyte, we find a first cycle irreversibility of ≈ 8%, which is a typical value for a high-quality anode active composite material with < 10 wt-% of silicon.

Determination of $V_{\mathrm{ElectrolyteLost}}$.- FEC is the only SEI forming additive in our electrolyte formulation. In a study by Jung et al.,[5] NMR analysis of extracted electrolyte revealed that FEC reduction takes place at a ratio of ≈ 4 e^-/FEC-molecule. Assuming that the entire $Q_{\mathrm{Irrev.FullCell}}$ is associated with FEC reduction due to its comparably high reduction potential,[6] we can calculate the amount of consumed FEC $n(FEC)_{\mathrm{lost}}$ according to

$$n(FEC)_{\mathrm{Lost}} = \frac{Q_{\mathrm{Irrev.SEI}}}{4F} \tag{S1}$$

where F is the Faraday constant. We find that $n(FEC)_{\mathrm{lost}}$ amounts to roughly 50% of the total FEC amount in the electrolyte and therefore it is a reasonable assumption that FEC reduction is the only process taking place at a significant rate during formation. This simplifies the further estimations as only one reaction has to be considered and not a combination of various reduction reactions.

To calculate the volume of lost electrolyte $V_{\mathrm{ElectrolyteLost}}$, we assumed that the electrolyte volume is a simple addition of the volumes of the individual electrolyte solvents and the liquid FEC additive, whereas the conducting salt $LiPF_6$ as solute does not add any volume. This assumption is justified as the electrolyte density calculated this way perfectly matches the actual electrolyte density. $V_{\mathrm{ElectrolyteLost}}$ can then be calculated in a straightforward way according to

$$V_{\mathrm{ElectrolyteLost}} = \frac{n(FEC)_{lost} M(FEC)}{\rho(FEC)} \tag{S2}$$

with $M(FEC)$ being the molar mass and $\rho(FEC)$ being the density of FEC.

The liquid electrolyte volume $V_{\mathrm{Electrolyte}}$ which remains in the cell after cell formation then equals

$$V_{\mathrm{Electrolyte}} = V_{\mathrm{ElectrolyteFilling}} - V_{\mathrm{ElectrolyteLost}} \tag{S3}$$

where $V_{\mathrm{ElectrolyteFilling}}$ is the electrolyte volume which is filled into the cell during production.

Determination of V(SEI). - The SEI volume is calculated according to

$$V(SEI) = \frac{m(SEI)}{\rho(SEI)} \quad \text{(S4)}$$

where *m(SEI)* is the mass and *ρ(SEI)* is the density of the SEI.

Let us first consider the mass of the SEI. The above cited study of Jung et al.[5] used online electrochemical mass spectrometry (OEMS) to show that FEC reduction releases as the only gaseous products one molecule of CO_2 per molecule of FEC and minor amounts of hydrogen. These experiments were carried out in a dedicated OEMS laboratory cell which is designed in such a way as to facilitate the transfer of released gases into the head space for detection. In contrast, in a 4695 cell any gas formed at the anode is trapped within the jelly roll and has to cover a distance of several centimeters before it can escape into the head space. This is especially difficult for CO_2 which is known to undergo further reactions at the anode, leading to an incorporation of the CO_2 into the anode SEI in the 4695 cell.[6] This is very useful for our estimation as this means that the entire mass of decomposed FEC is ending up in the SEI (except for minor amounts hydrogen which can be neglected due to its low molecular weight). The SEI weight *m(SEI)* can therefore be calculated according to

$$m(SEI) = n(FEC)_{loss} \cdot (M(FEC) + 4 \cdot M(Li)) \quad \text{(S5)}$$

where *M(Li)* is the molar mass of lithium; the term $4 \cdot M(Li)$ in equation S5 reflects the fact that every FEC molecule takes up 4 electrons from the anode active material (as discussed above), which must be accompanied by the same number of lithium-ions to maintain charge neutrality. Based on these assumptions, one can calculate the ratio of SEI mass to SEI charge to equal 1.25 mg(SEI)/mAh(SEI). This agrees well with preliminary experimental data which will be presented in detail in a separate study. For the present manuscript we prefer to rely on this stand-alone first principles model to estimate the SEI mass.

Now, the only value still missing to calculate the SEI volume is the SEI density *ρ(SEI)*. As the FEC SEI is a mixture of LiF and polymeric species of unknown chemical structure[6] it is not straightforward to estimate an average SEI density based on theoretical considerations as done above for *m(SEI)*. We therefore use a SEI density *ρ(SEI)* of 1.6 g/cm^3 which has been independently determined by helium pycnometer by our group and also by Lennart Reuter and co-workers (Technical University of Munich, group of Prof. Hubert Gasteiger).

Influence of $V_{\text{ElectrolyteLost}}$ and V(SEI) on the pore filling ratio. - Using the model approach outlined above and equations S2 and S3, we find that $V_{ElectrolyteLost}$ and *V(SEI)* both equal ≈ 2 mL for our 4695 cell chemistry. At first glance this might be counter-intuitive as one might expect the "disappearing" liquid electrolyte to have a lower density and therefore higher volume than the "emerging" solid SEI, but the difference in density between FEC and SEI is minor (1.49 vs 1.60 g/cm^3) and the four lithium-ions per FEC-molecule add "extra weight" and volume to the SEI. This means that the effects of $V_{\text{ElectrolyteLost}}$ and *V(SEI)* roughly cancel out when calculating the pore filling ratio. It is important to keep in mind though, that this is only valid for the combination of anode active material and electrolyte used in this study. For other electrolyte or anode active material formulations, the ratio of $V_{\text{ElectrolyteLost}}$ and *V(SEI)* might very well be significantly different.

When comparing the ≈ 2 mL to the total jelly pore volume (sum of anode, cathode and separator porosity) of ≈ 35 mL at 100% SOC (see Figure 1c) we find that both $V_{\text{ElectrolyteLost}}$ and *V(SEI)* would individually alter the pore filling ratio by ≈ 0.06 (= 2 / 35), which is not insignificant given the necessary precision to differentiate between cells which do or do not generate free electrolyte.

Moment of inertia measurements

Experimental Setup. - Figure S1 shows the experimental setup used to measure the moment of inertia of the 4695 cells.

Figure S1 Experimental set-up used for measuring the moment of inertia of 4695 cells.

Non-zero moment of inertia change of low-electrolyte cell. - In the main manuscript, the influence of electrolyte motion on the moment of inertia of a lithium-ion cell was discussed. Here we briefly discuss possible jelly-roll *internal* electrolyte distributions for cells with a pore filling ratio $PFR < 1.0$ to rationalize the non-zero moment of inertia change of the low electrolyte cells (see Figures 3c-e of main manuscript). In the main manuscript, all pore filling ratios are average values in the sense that a given cell has exactly one *PFR* value per SOC (see equation 2 in main manuscript). Here, we rename this average value PFR_{global} to distinguish it from the local pore filling ratio PFR_{local} which we introduce to describe scenarios of uneven electrolyte distribution within the jelly roll (JR).

Figure S2 shows three different conceivable jelly roll internal electrolyte distribution scenarios for low electrolyte cells (Figures S2b, c and d) and one single scenario for a high electrolyte cell (Figure S2a). For the high electrolyte cell displayed in Figure S2a ($PFR_{global} = 1$ at 0% SOC), the jelly roll porosity is fully filled with electrolyte at 0 and 100% SOC and the moment of inertia increases during charging and returns to its original value at the end of the following discharge. We believe that the high electrolyte cells displayed in Figure 3 (main manuscript) behave in such a way.

For the low electrolyte cells, we start by looking at the case when the electrolyte is uniformly distributed through the length of the jelly roll at 0% SOC ($PFR_{global} = PFR_{local} = 0.8$) as shown in Figure S2b and c. On charging, the jelly roll porosity contracts, and the electrolyte uniformly occupies the whole jelly roll ($PFR_{global} = PFR_{local} = 1.0$). Since there is no overflow of the electrolyte into the donut volume (DV) and the electrolyte remains uniformly distributed, there will be no change in the moment of inertia. Thus, in Figure 2 b and c the moment of inertia remains constant upon charging $I_0 \approx I_{100}$.

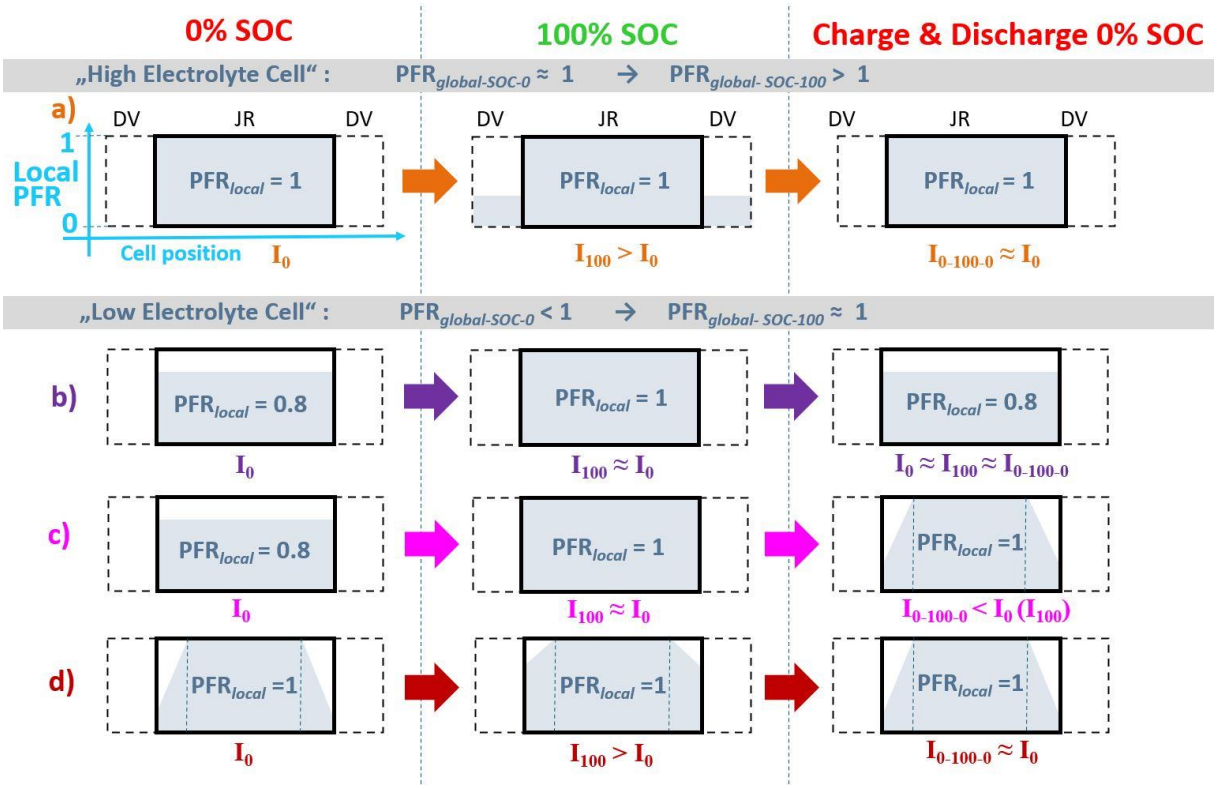

Figure S2 Some possible scenarios of electrolyte distribution within jelly roll (JR) and donut volume (DV) for a) high electrolyte cells and b-d) low electrolyte cells. Each diagram corresponds to a 4695 cell in horizontal orientation and is divided into the main jelly roll pore volume (JR – central rectangle) and the free space in the donut volume (DV - dashed rectangles). The y-axis of each cell diagram corresponds to the pore filling ratio (PFR), the ratio of free space in the region of the cell and the electrolyte volume filling it.

Two possible scenarios could occur on the following discharge. The first (Figure S2 b) is that, as the cell discharges, the pore filling level decreases uniformly across the entire jelly roll to a value of $PFR_{global} = PFR_{local} = 0.8$, and thus - once again - the moment of inertia of the cell would not change $I_0 \approx I_{100} \approx I_{0\text{-}100\text{-}0}$, as no electrolyte motion occurs during charging or discharging. Such a scenario might arise if gas from outside the jelly roll would be able to infiltrate the entire jelly roll fast enough.

Another possible scenario is presented in Figure S2 c, where on discharge the center of the jelly roll remains fully filled with $PFR_{local} = 1$ and the PFR_{local} drops around the edges of the jelly roll. This case (right column diagram in Figure S2 c), would result in a decrease of the moment of inertia on discharge, compared to the initial SOC 0% I_0 and the charged I_{100}, i.e., $I_{0\text{-}100\text{-}0} < I_0$ (and $I_{0\text{-}100\text{-}0} < I_{100}$).

The last case we wish to discuss here addresses the cell configuration in which the electrolyte distribution within the jelly roll is not uniform at the initial 0% SOC, with higher PFR_{local} at the center and decreasing PFR_{local} values towards the edges (Figure S2 d). In this case, the moment of inertia will behave qualitatively similarly to the high electrolyte cell. The moment of inertia at 100% SOC charge will increase ($I_{100} > I_0$) and then drop back down to lower values on discharge ($I_{0\text{-}100\text{-}0} \approx I_0$). At this point it is important to note that the magnitude of the moment of inertia change is not only proportional to the mass of electrolyte moved, but also to the *distance* which it is moved *from the center of the cell* (the point where the moment of inertia is measured). The increase in the cell's moment of inertia in the case described above will therefore *not be as large* compared to a cell where the *same amount of electrolyte is pushed further* out into the DV (Figure S2 a).

The behavior described in Figure S2 d might be responsible for the low but non-zero moment of inertia change observed for the low electrolyte cell (main manuscript Figure 3), but further research is needed

to gain better understanding of electrolyte distribution in lithium-ion cells with partial pore filling. It is important to note that the scenarios depicted in Figure S2 are simplifications of real electrolyte distributions and incomplete as many other scenarios are conceivable.

Fast-charging procedure

Fast charging from 10 to 80% SOC was carried out at a ambient (= initial) temperature of 35 °C and with a fast charge time of 16 to 21 minutes (exact charging time cannot be disclosed). An industry standard step current profile was used with an initial C-rate of ≈ 3C (exact C-rate cannot be disclosed); with increasing SOC the C-rate is reduced to prevent lithium plating (blue line in Figure S3). Details on the design and rational of such current profiles is explained in detail in our previous publications.[7,8] The temperature (measured on the cell housing) increases rapidly and peaks at around 55 °C (red line in Figure S3). This temperature increase is beneficial as it increases mass transport and therefore prevents lithium plating.

The fast charge half-cycle shown in Figure S3 represents an early cycle; upon aging, the voltage and temperature curves gradually shift upwards due to increasing cell resistance. The fast charge time is not affected though, as the current steps are controlled via charge throughput and not via cell potential under load as is also sometimes done.

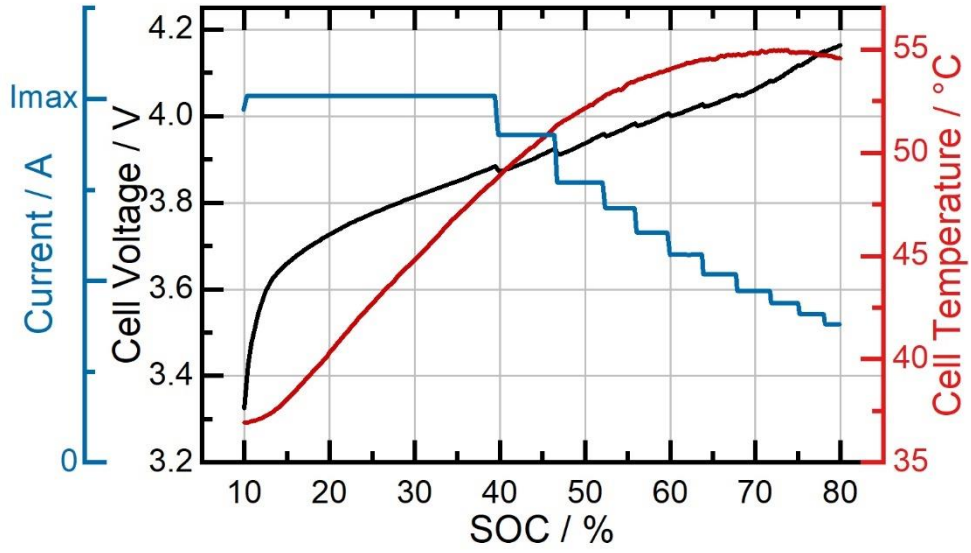

Figure S3 Current (blue), cell voltage (black) and cell temperature (red) versus SOC during fast charge of a 4695 cell as used in this study.

Sampling of electrode coins

Figures S4 a and b give an overview of location and diameter of electrode coins punched out from unrolled jelly rolls for analysis via LC-MS (blue) and IC (green). Figure S4 a and b display an idealized sampling pattern, in reality minor deviations from the intended positions were unavoidable, especially for aged jelly rolls.

For every IC and LC-MS sampling positions (top/middle/bottom), the z-axis position value (Figure S4 c) was defined as the distance from the lower electrode edge to the center of each electrode coin. Due to different electrode coins sizes, the three sampling positions give five different z-axis values. The two outermost positions are sampled by IC only ($z \approx 7$ & 73 mm), the two second-outermost ($z \approx 13$ & 67 mm) are sampled by LC-MS only and the center position ($z \approx 40$ mm) is sampled by both IC and LC-MS.

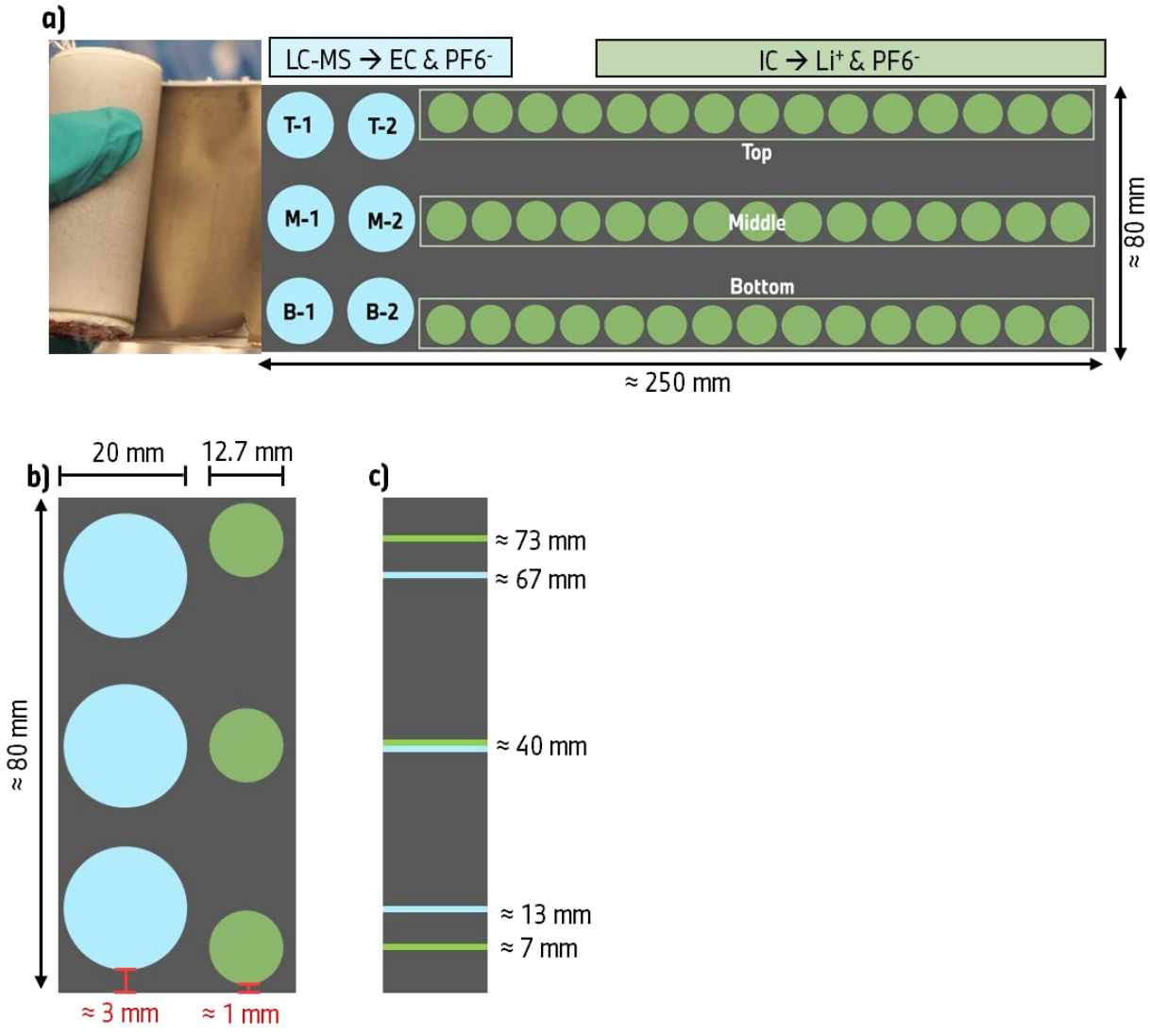

Figure S4 Sampling of electrode coins for LC-MS (blue) and IC (green) analysis; a) overview of sampling position, b) diameter and distance from coating edge and c) y-axis value of each sample.

Determination of electrolyte solvent distribution

In an initial experiment, the time-dependency of *α(EC)* and *α(DMC)* was investigated (Figure S5) for a BOL cell. In contrast to Figure 6 of the main manuscript, the *α(solvent)* values are shown without z-axis resolution in Figure S4. For the BOL cell, all three z-axis positions (top/middle/bottom) give very similar values and are therefore averaged into a single value.

In this initial experiment, special care was taken to i) execute the unrolling of the jelly roll and sampling of electrode coins as quickly as possible and ii) to exactly record the time available for solvent evaporation. Solvent evaporation started once the respective part of the jelly roll from which electrode coins were sampled was unrolled, this is t = 0 s in Figure S5. The data points at t = 0 s are not measured values but are by definition set to 100%. After unrolling of the jelly roll (t= 0 s), one 20 mm coin was punched in top, middle and bottom position each (T1, M1 and B1 in Figure S4) and these three coins were dropped into three plastic vials filled with acetonitrile after ≈ 80 s of evaporation time; three other samples (T2, M2, B2) were dropped into acetonitrile after ≈ 260 s of evaporation time.

For EC, all *α(EC)* values were close to 100%, showing no significant downward trend over time and small error bars, which indicates that the EC determination is robust. For DMC, already the initial *α(DMC)* value after 80 s is very low (≈ 43%) and exhibits a large standard deviation. Therefore, *α(DMC)* is extremely sensitive towards the time it takes to punch out electrode coins (= evaporation time) and is not further considered in this manuscript. For a proper assessment of *α(DMC)*, it will probably be necessary to develop a new method in which the electrodes are frozen during cell opening to prevent any solvent evaporation, but this is beyond the scope of the current manuscript.

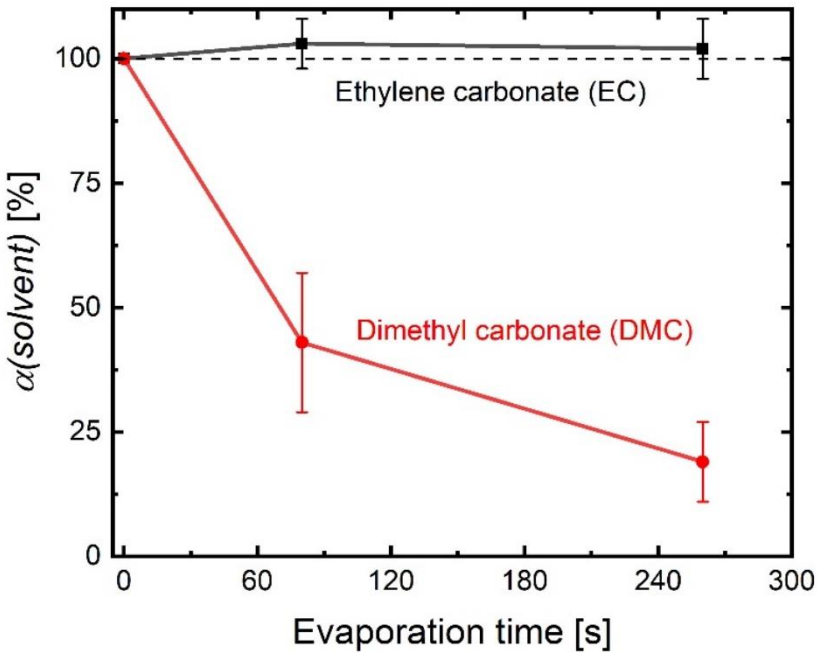

Figure S5 Dependency of *α(EC)* and *α(DMC)* values on the evaporation time (= time between unrolling of jelly roll and dropping of electrode coin into a plastic vial) for a BOL cell; all electrode coins were sampled from a cathode; error bars indicate standard deviation of top, middle, and bottom positions.

LC-MS analysis of $LiPF_6$ concentrations for 130 cycle cells

In Figure 6 of the main manuscript, the two second outer-most $LiPF_6$ concentration values are missing for cells cycled for 130 cycles. As explained in detail in the Methods Section, this is because a LC-MS calibration curve is missing which makes it impossible to quantify $LiPF_6$ amounts in units of mol/L for all LC-MS $LiPF_6$ samples for these 130 cycle cells.

The missing LC-MS $LiPF_6$ concentrations for the 130 cycle high electrolyte cells are displayed in Figure S6, referenced to the center position which is set to 100%. These normalized LC-MS $LiPF_6$ concentrations (in units of %) are shown in brown color and are plotted against the upper x-axis. The $LiPF_6$ concentrations sampled by IC (in units of mol/L_{pore}) is shown in red color and plotted against the lower x-axis. The IC data (red symbols and lines) are fully identical to the data displayed in Figures 6 c to e of the main manuscript. The upper x-axis is scaled in such a way that the center positions are overlapping for the LC-MS and IC LiPF6 concentrations. As can be seen in Figure S6, the LC-MS data matches to the $LiPF_6$ concentration profiles as determined by IC.

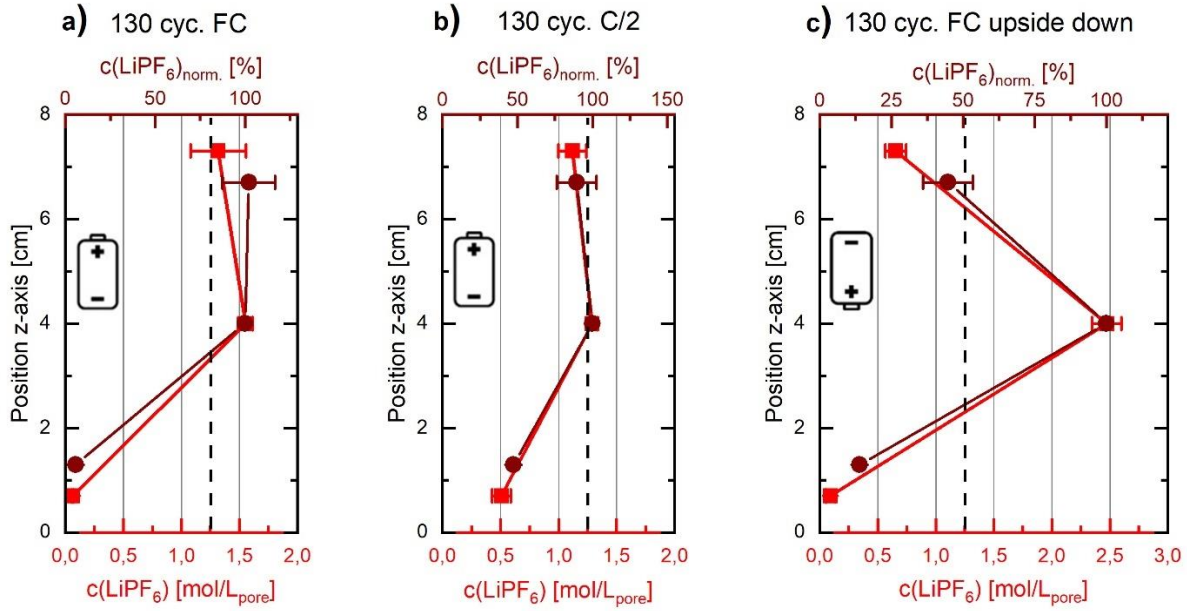

Figure S6 Comparison of LC-MS $LiPF_6$ concentration after normalization to center position (brown symbols and lines, upper x-axis) in units of % with the IC $LiPF_6$ concentrations in units of mol/L_{pore} (red symbols and lines, lower x-axis) for the high electrolyte cells after 130 cycles for a) fast charge with the positive terminal facing up, b) C/2 cycling with the positive terminal facing up and c) fast charge with the positive terminal facing down. The IC data (red symbols and lines) is identical to the data presented in Figures 6 c to e in the main manuscript.

$LiPF_6$ and α(EC) values

In Table S1 and S2, we summarize the $LiPF_6$ concentrations and *α(EC)* values displayed in Figure 6 of the main manuscript. As explained in detail in the Methods Section, the absolute values (4th column in Table S1 and Table S2) might contain a systematic error due to the pore volume calculation which is not captured by the standard deviation while the relative trend between different samples should be very robust. For each cycling condition, two reproduced and nominally identical cells were analyzed.

Table S1 $LiPF_6$ concentrations (referenced to the pore volume) determined in electrodes sampled from BOL and cycled 4695 cells.

Test case	Electrolyte amount	Position [cm]	c(LiPF6) [mol/L_{pore}]	Analytical technique	Electrode sampled	# of samples
BOL	High	7.3	0.86 ± 0.19	IC only	An + Ca	4
		6.7	1.19 ± 0.07	LC-MS only	An + Ca	8
		4.0	1.23 ± 0.07	IC + LC-MS	An + Ca	12
		1.3	1.25 ± 0.09	LC-MS only	An + Ca	8
		0.7	1.36 ± 0.18	IC only	An + Ca	4
BOL	Low	7.3	1.01 ± 0.08	IC only	An + Ca	4
		6.7	1.09 ± 0.07	LC-MS only	An + Ca	8
		4.0	1.10 ± 0.09	IC + LC-MS	An + Ca	12
		1.3	1.02 ± 0.05	LC-MS only	An + Ca	8
		0.7	0.99 ± 0.12	IC only	An + Ca	4
18 cycles FC positive terminal up	High	7.3	0.98 ± 0.03	IC only	An + Ca	4
		6.7	1.35 ± 0.06	LC-MS only	An + Ca	8
		4.0	1.70 ± 0.12	IC + LC-MS	An + Ca	12
		1.3	0.92 ± 0.07	LC-MS only	An + Ca	8
		0.7	0.52 ± 0.05	IC only	An + Ca	4
18 cycles FC positive terminal up	Low	7.3	0.89 ± 0.10	IC only	An + Ca	4
		6.7	1.04 ± 0.11	LC-MS only	An + Ca	8
		4.0	1.14 ± 0.12	IC + LC-MS	An + Ca	12
		1.3	1.08 ± 0.08	LC-MS only	An + Ca	8
		0.7	0.92 ± 0.12	IC only	An + Ca	4
130 cyc FC positive terminal up	High	7.3	1.32 ± 0.24	IC only	Ca	2
		4.0	1.55 ± 0.06	IC only	Ca	2
		0.7	0.06 ± 0.01	IC only	Ca	2
130 cyc FC positive terminal up	Low	7.3	0.87 ± 0.00	IC only	Ca	2
		4.0	1.23 ± 0.05	IC only	Ca	2
		0.7	0.78 ± 0.02	IC only	Ca	2
130 cyc FC positive terminal down	High	7.3	0.65 ± 0.09	IC only	Ca	2
		4.0	2.47 ± 0.13	IC only	Ca	2
		0.7	0.09 ± 0.04	IC only	Ca	2
130 cyc FC positive terminal down	Low	7.3	0.93 ± 0.04	IC only	Ca	2
		4.0	1.22 ± 0.07	IC only	Ca	2
		0.7	0.94 ± 0.00	IC only	Ca	2
130 cyc 0.5C positive terminal up	High	7.3	1.12 ± 0.12	IC only	Ca	2
		4.0	1.29 ± 0.04	IC only	Ca	2
		0.7	0.51 ± 0.08	IC only	Ca	2
130 cyc 0.5C positive terminal up	Low	7.3	1.03 ± 0.02	IC only	Ca	2
		4.0	1.14 ± 0.06	IC only	Ca	2
		0.7	1.06 ± 0.04	IC only	Ca	2

Table S2 *α(EC)* values determined in electrodes sampled from BOL and cycled 4695 cells.

Test case	Electrolyte amount	Position [cm]	*α(EC)* [%]	Analytical technique	Electrode sampled	# of samples
BOL	High	6.7	113 ± 6	LC-MS only	An + Ca	8
		4.0	116 ± 10	LC-MS only	An + Ca	8
		1.3	122 ± 17	LC-MS only	An + Ca	8
BOL	Low	6.7	106 ± 10	LC-MS only	An + Ca	8
		4.0	106 ± 9	LC-MS only	An + Ca	8
		1.3	106 ± 9	LC-MS only	An + Ca	8
18 cycles FC positive terminal up	High	6.7	115 ± 8	LC-MS only	An + Ca	8
		4.0	111 ± 9	LC-MS only	An + Ca	8
		1.3	107 ± 7	LC-MS only	An + Ca	8
18 cycles FC positive terminal up	Low	6.7	92 ± 11	LC-MS only	An + Ca	8
		4.0	90 ± 12	LC-MS only	An + Ca	8
		1.3	90 ± 8	LC-MS only	An + Ca	8
130 cyc FC positive terminal up	High	6.7	114 ± 17	LC-MS only	Ca	4
		4.0	121 ± 10	LC-MS only	Ca	4
		1.3	62 ± 6	LC-MS only	Ca	4
130 cyc FC positive terminal up	Low	6.7	106 ± 6	LC-MS only	Ca	4
		4.0	102 ± 4	LC-MS only	Ca	4
		1.3	106 ± 4	LC-MS only	Ca	4
130 cyc FC positive terminal down	High	6.7	120 ± 5	LC-MS only	Ca	4
		4.0	115 ± 6	LC-MS only	Ca	4
		1.3	82 ± 7	LC-MS only	Ca	4
130 cyc FC positive terminal down	Low	6.7	90 ± 13	LC-MS only	Ca	4
		4.0	86 ± 14	LC-MS only	Ca	4
		1.3	88 ± 19	LC-MS only	Ca	4
130 cyc C/2 positive terminal up	High	6.7	118 ± 4	LC-MS only	Ca	4
		4.0	121 ± 7	LC-MS only	Ca	4
		1.3	104 ± 5	LC-MS only	Ca	4
130 cyc C/2 positive terminal up	Low	6.7	100 ± 11	LC-MS only	Ca	4
		4.0	99 ± 7	LC-MS only	Ca	4
		1.3	106 ± 10	LC-MS only	Ca	4

Cycling data

Tables S3-S5 contain the electrochemical cycling data shown in Figure 4 of the main manuscript. Table S3 shows C/3 discharge capacity and DCIR at 50%, 80% and 20% SOC from the reference performance test (RPTs) at 25 °C which was performed after each 48th cycle as well as at the end of the cycling tests. Table S4 shows the discharge endpoint slippage, normalized to the initial cell capacity, after each 6th cycle during cycling at 35 °C. Table S5 shows the average discharge voltage (calculated as discharge energy divided by discharge capacity) during the first discharge of each 3x C/2/C/2 + 3x FC/C2 sequence during cycling at 35 °C. Two nominally identical cells were cycled for each condition and their normalized values were averaged. Error values represent the min/max deviation from the average.

Table S3 C/3 discharge capacity and DCIR at 50% SOC, 80% SOC, 20% SOC from reference performance tests (RPT) at 25 °C

Test case	Electrolyte amount	Cycle Number	C/3 Capacity [%]	DCIR 50% SOC [%]	DCIR 80% SOC [%]	DCIR 20% SOC [%]
Fast charge positive terminal up	High	0	100 ± 0	100 ± 0	100 ± 0	100 ± 0
		48	93.3 ± 0.3	118.4 ± 1.3	117.3 ± 1.1	116 ± 0.8
		96	81.5 ± 1	141.8 ± 2.2	139.5 ± 2	128.9 ± 1
		126	76.5 ± 0.7	151.1 ± 1.9	148.9 ± 1.8	136.9 ± 1.4
Fast charge positive terminal up	Low	0	100 ± 0	100 ± 0	100 ± 0	100 ± 0
		48	98.6 ± 0	100.6 ± 0.6	101.5 ± 0.6	98.6 ± 0.3
		96	96.9 ± 0.1	102.2 ± 0.7	103.7 ± 0.6	99.1 ± 0.4
		132	95.2 ± 0.1	104.2 ± 0.9	106.2 ± 0.9	100.1 ± 0.6
C/2 positive terminal up	High	0	100 ± 0	100 ± 0	100 ± 0	100 ± 0
		48	98.9 ± 0	101.1 ± 0.5	101.8 ± 0.4	98.3 ± 0.3
		96	98 ± 0	102.3 ± 0.7	103.3 ± 0.7	98.5 ± 0.5
		128	97.5 ± 0	103.1 ± 0.8	104.3 ± 0.8	98.6 ± 0.5
C/2 positive terminal up	Low	0	100 ± 0	100 ± 0	100 ± 0	100 ± 0
		48	99.1 ± 0	99.9 ± 0.8	100.9 ± 0.7	97.2 ± 0.6
		96	98.5 ± 0.1	100 ± 0.8	101.5 ± 0.8	96.1 ± 0.6
		128	98.1 ± 0.1	100.1 ± 0.8	102 ± 0.7	95.4 ± 0.5
Fast charge positive terminal down	High	0	100 ± 0	100 ± 0	100 ± 0	100 ± 0
		48	95.1 ± 0.6	115.5 ± 1.2	115 ± 1.1	113.4 ± 0.9
		96	84.6 ± 1.9	136.1 ± 3.9	135.1 ± 3.5	124.8 ± 2.1
		128	79.6 ± 1.8	145 ± 3.5	144.6 ± 3.2	130.3 ± 2.4
Fast charge positive terminal down	Low	0	100 ± 0	100 ± 0	100 ± 0	100 ± 0
		48	98.5 ± 0.1	101.4 ± 0.8	102.4 ± 0.8	99.1 ± 0.9
		96	97.2 ± 0.4	102.7 ± 0.6	104.3 ± 0.6	99.1 ± 0.8
		132	95.9 ± 0.6	104.1 ± 0.4	106.3 ± 0.5	99.7 ± 0.7
Fast charge positive terminal up	High	0	100 ± 0	100 ± 0	100 ± 0	100 ± 0
		48	94 ± 0.3	N/A	N/A	N/A
		48 + 50 h storage	98.2 ± 0.2	99.7 ± 0.8	100.6 ± 0.7	99.3 ± 1.2
Fast charge positive terminal up	Low	0	100 ± 0	100 ± 0	100 ± 0	100 ± 0
		48	99.1 ± 0.1	N/A	N/A	N/A
		48 + 50 h storage	99.9 ± 0.1	97.1 ± 0.6	98.9 ± 0.7	96.5 ± 0.4

Table S4 Discharge endpoint slippage [%] normalized by initial cell capacity after each 3x C/2/C/2 + 3x FC/C2 sequence during cycling at 35 °C. As the lower SOC during cycling was 10%, all cells show an initial offset of ~10%.

Cycle Nr.	**Fast charge positive terminal up**		**C/2 positive terminal up**		**Fast charge positive terminal down**	
Electrolyte amount	**High**	**Low**	**High**	**Low**	**High**	**Low**
6	10 ± 0	9.7 ± 0	10 ± 0	9.5 ± 0.1	9.9 ± 0.1	9.7 ± 0.1
12	11.1 ± 0.1	10.9 ± 0.1	11 ± 0	10.6 ± 0.1	11 ± 0	10.9 ± 0.1
18	11.9 ± 0.1	11.5 ± 0	11.6 ± 0	11.3 ± 0.1	11.9 ± 0.1	11.6 ± 0.1
24	12.6 ± 0	11.9 ± 0	12.1 ± 0	11.6 ± 0.1	12.7 ± 0.3	12 ± 0.1
30	13.3 ± 0	12.2 ± 0	12.4 ± 0	11.9 ± 0.1	13.4 ± 0.4	12.3 ± 0.1
36	14 ± 0	12.5 ± 0	12.7 ± 0	12.2 ± 0.1	14.1 ± 0.4	12.6 ± 0.1
42	14.7 ± 0.1	12.7 ± 0	12.9 ± 0	12.4 ± 0.1	14.7 ± 0.5	12.8 ± 0.1
48	15.5 ± 0.1	12.9 ± 0	13.3 ± 0	12.7 ± 0.1	15.5 ± 0.5	13 ± 0.1
54	14.5 ± 0.1	11.5 ± 0	11.6 ± 0	11 ± 0.1	14.2 ± 0.7	11.6 ± 0.1
60	15.7 ± 0.2	12.5 ± 0.1	12.5 ± 0	12 ± 0.1	15.8 ± 0.7	12.5 ± 0.1
66	16.6 ± 0.2	13.1 ± 0.1	13 ± 0	12.5 ± 0.1	17 ± 0.7	13 ± 0.1
72	17.4 ± 0.3	13.4 ± 0.1	13.3 ± 0	12.8 ± 0.1	17.9 ± 0.8	13.4 ± 0.1
78	18.2 ± 0.3	13.7 ± 0.1	13.6 ± 0	13 ± 0.1	18.6 ± 0.8	13.6 ± 0
84	18.9 ± 0.3	14 ± 0.1	13.8 ± 0	13.1 ± 0.1	19.3 ± 0.9	13.9 ± 0
90	19.6 ± 0.2	14.2 ± 0.1	14 ± 0	13.3 ± 0.1	20 ± 0.9	14.1 ± 0.1
96	20.2 ± 0.2	14.5 ± 0.1	14.1 ± 0	13.4 ± 0.1	20.6 ± 1	14.4 ± 0.1
102	19.5 ± 0.3	13.1 ± 0.1	12.7 ± 0	11.9 ± 0.1	19.2 ± 1.2	13 ± 0.1
108	20.2 ± 0.3	14 ± 0.1	13.5 ± 0	12.8 ± 0.1	20.4 ± 1	13.9 ± 0
114	20.8 ± 0.3	14.5 ± 0.1	14 ± 0	13.2 ± 0.1	21.2 ± 1	14.4 ± 0
120	21.5 ± 0.3	14.8 ± 0.1	14.2 ± 0	13.5 ± 0.1	21.9 ± 1	14.8 ± 0
126	22.1 ± 0.3	15.1 ± 0.1	14.4 ± 0	13.7 ± 0.1	22.4 ± 1	15.1 ± 0.1
132	N/A	15.4 ± 0.1	N/A	N/A	N/A	15.4 ± 0.1

Table S5 Average discharge voltage (calculated from discharge energy / discharge capacity) from the first discharge of each 3x C/2/C/2 + 3x FC/C2 sequence during cycling at 35 °C

Cycle Nr.	**Fast charge positive terminal up**		**C/2 positive terminal up**		**Fast charge positive terminal down**	
Electrolyte amount	**High**	**Low**	**High**	**Low**	**High**	**Low**
1	3.735 ± 0	3.735 ± 0	3.735 ± 0	3.735 ± 0.001	3.736 ± 0.001	3.735 ± 0.001
7	3.739 ± 0.001	3.741 ± 0.001	3.739 ± 0	3.74 ± 0.001	3.739 ± 0.001	3.741 ± 0.001
13	3.74 ± 0.001	3.744 ± 0.001	3.743 ± 0.001	3.743 ± 0.001	3.741 ± 0.002	3.744 ± 0.001
19	3.74 ± 0.001	3.745 ± 0.001	3.745 ± 0.001	3.744 ± 0.001	3.741 ± 0.002	3.745 ± 0.001
25	3.739 ± 0.001	3.745 ± 0.001	3.745 ± 0.001	3.745 ± 0.001	3.74 ± 0.002	3.746 ± 0.001
31	3.736 ± 0.001	3.746 ± 0.001	3.746 ± 0.001	3.745 ± 0.001	3.738 ± 0.002	3.746 ± 0.001
37	3.734 ± 0.001	3.745 ± 0.001	3.746 ± 0.001	3.746 ± 0.001	3.736 ± 0.002	3.746 ± 0.001
43	3.731 ± 0	3.745 ± 0.001	3.747 ± 0.001	3.746 ± 0.001	3.733 ± 0.002	3.746 ± 0.001
49	3.727 ± 0.001	3.735 ± 0.001	3.735 ± 0.001	3.735 ± 0.001	3.729 ± 0.002	3.735 ± 0.001
55	3.726 ± 0.001	3.741 ± 0.001	3.739 ± 0.001	3.741 ± 0.002	3.728 ± 0.003	3.741 ± 0.001
61	3.724 ± 0.001	3.743 ± 0.001	3.743 ± 0.001	3.744 ± 0.002	3.727 ± 0.003	3.743 ± 0.001
67	3.722 ± 0.001	3.744 ± 0.001	3.744 ± 0.001	3.745 ± 0.002	3.724 ± 0.003	3.744 ± 0.001
73	3.72 ± 0.001	3.743 ± 0.001	3.745 ± 0.001	3.745 ± 0.002	3.722 ± 0.004	3.744 ± 0.001
79	3.717 ± 0.001	3.743 ± 0.001	3.745 ± 0.001	3.746 ± 0.001	3.719 ± 0.004	3.744 ± 0.001
85	3.715 ± 0.001	3.743 ± 0.001	3.745 ± 0.001	3.746 ± 0.001	3.717 ± 0.004	3.744 ± 0.001
91	3.713 ± 0.001	3.742 ± 0.001	3.746 ± 0.001	3.746 ± 0.001	3.715 ± 0.004	3.74 ± 0.001
97	3.714 ± 0.002	3.734 ± 0.001	3.735 ± 0.001	3.736 ± 0.001	3.717 ± 0.003	3.734 ± 0.001
103	3.711 ± 0.001	3.739 ± 0.001	3.739 ± 0.001	3.741 ± 0.002	3.713 ± 0.004	3.739 ± 0.002
109	3.709 ± 0.001	3.741 ± 0.001	3.742 ± 0.001	3.744 ± 0.002	3.711 ± 0.004	3.741 ± 0.002
115	3.707 ± 0.001	3.741 ± 0.001	3.743 ± 0.001	3.745 ± 0.002	3.708 ± 0.004	3.742 ± 0.002
121	3.705 ± 0.001	3.741 ± 0.001	3.744 ± 0.001	3.746 ± 0.002	3.706 ± 0.004	3.742 ± 0.002
127	N/A	3.741 ± 0.001	3.744 ± 0.001	3.746 ± 0.002	3.704 ± 0.004	3.742 ± 0.002

References

1 S. J. An, J. Li, D. Mohanty, C. Daniel, B. J. Polzin, J. R. Croy, S. E. Trask and D. L. Wood, *J. Electrochem. Soc.*, 2017, **164**, A1195-A1202.

2 F. J. Günter, C. Burgstaller, F. Konwitschny and G. Reinhart, *J. Electrochem. Soc.*, 2019, **166**, A1709.

3 H. Pegel, O. von Kessel, P. Heugel, T. Deich, J. Tübke, K. P. Birke and D. U. Sauer, *Journal of Power Sources*, 2022, **537**, 231443.

4 D. Vidal, C. Leys, B. Mathieu, N. Guillet, V. Vidal, D. Borschneck, P. Chaurand, S. Genies, E. de Vito, M. Tulodziecki and W. Porcher, *Journal of Power Sources*, 2021, **514**, 230552.

5 R. Jung, M. Metzger, D. Haering, S. Solchenbach, C. Marino, N. Tsiouvaras, C. Stinner and H. A. Gasteiger, *J. Electrochem. Soc.*, 2016, **163**, A1705-A1716.

6 K. U. Schwenke, S. Solchenbach, J. Demeaux, B. L. Lucht and H. A. Gasteiger, *J. Electrochem. Soc.*, 2019, **166**, A2035-A2047.

7 A. Adam, K. Huber, E. Knobbe, D. Grießl, J. Wandt and A. Kwade, *Journal of Power Sources*, 2021, **512**, 230469.

8 A. Adam, E. Knobbe, J. Wandt and A. Kwade, *Journal of Power Sources*, 2021, **495**, 229794.